Computers and Geotechnics 62 (2014) 128–135

Contents lists available at ScienceDirect

Computers and Geotechnics

journal homepage: www.elsevier.com/locate/compgeo

Technical Communication

Undrained stability of surface strip footings above voids

Joon Kyu Lee, Sangseom Jeong *, Junyoung Ko

Dept. of Civil and Environmental Engineering, Yonsei University, 50 Yonsei-ro, Seodaemun-gu, Seoul 120-749, Republic of Korea

ARTICLE INFO

Article history:
Received 27 May 2014
Received in revised form 23 June 2014
Accepted 8 July 2014

Keywords:
Strip footing
Void
Finite element analysis
Undrained bearing capacity
Clay

ABSTRACT

This paper investigates the undrained vertical bearing capacity of surface strip footings on clay with single and dual continuous voids. Numerical solutions for a wide range of geometric and material combinations are obtained by small strain finite element analysis. Based on the results, design charts are provided for the calculation of the undrained bearing capacity factors as a function of the dimensionless parameters related to the vertical and horizontal void distances from the footing, void width and height, and spacing between the two voids as well as soil rigidity and non-homogeneity. In the footing-above-void system, the ultimate bearing capacity of the footing is governed by the three failure mode: roof, wall, and combined failure mechanisms.

1. Introduction

In engineering practice, the existence of underground voids under rigid surface structures (e.g., pavements, pipelines and footings) requires special attention because voids can influence the integrity of structures. Voids in ground are known to form for many reasons, some of which are the thawing of subsurface ice lenses [1], the dynamic loadings induced by mining and tunneling activities [2], the dissolution of soluble materials such as salt, gypsum, limestone and dolomite [3], the dissociation of methane hydrate [4], and the presence of leaking CO_2 storage reservoirs [5]. The size, shape and evolution of voids depend on the lithology of soils and rocks, and the initial depth of voids [6]. In particular, large voids are often found in karstic environment [7].

The performance of footings underlain by subsurface voids has been investigated by several researchers. Baus and Wang [8] studied experimentally and numerically the bearing capacity behavior of strip footings on silty clay with single continuous voids, and showed that for a given void size, the bearing capacity decreases as the distance between the footing and void reduces. Wang and his colleagues continuously explored the effects of void location, size, shape, and orientation with respect to the footing axis on the stability of square footings with different sizes, shapes and embedment depths [9,10]. Wood and Larnach [11] conducted another study on this subject by using physical modeling and numerical simulation, and reported similar behaviors observed in Wang's works. Wang and Hsieh [12] developed the three failure mechanisms that are considered to model the collapse of strip footing centered above a single circular void by using the upper bound theorem of limit analysis. Al-Tabbaa et al. [13] observed the load-settlement characteristics of model strip footings over continuous circular voids in cemented mixed sand. The results indicated that the greater depth and offset of voids cause the higher strength and stiffness of the system. Sreng et al. [14] presented the result of rotation response of strip footings above continuous square voids, which is obtained by measuring both vertical and horizontal displacements during 1 g model tests. More recently, Kiyosumi et al. [15] performed plain strain finite element (FE) analyses to examine the influence of multiple voids on the yield pressure of strip footing resting on calcareous soil, and stated that the failure zone developed significantly towards the nearest void from the footing and does not typically extend to the other voids. Kiyosumi et al. [16] reported the results of laboratory scale model tests of strip footing on stiff ground with continuous square voids and revealed the three types of collapse modes for a single void: bearing failure without void collapse, bearing failure with void collapse, and void failure without bearing failure. Even though several studies have been reported on the footing-above-void system, most works have focused on cohesive-frictional soils. In contrast, the undrained stability of footings overlying voids has not been discussed in the literature.

The bearing capacity of surface strip footings (both drained and undrained) is usually estimated using the bearing capacity formula suggested by Meyerhof [17]. The solution for the simplest case of undrained condition is identical to the exact solution of Prandtl [18], which is expressed as

* Corresponding author. Tel.: +82 2 2123 2807; fax: +82 2 364 5300.
E-mail address: soj9081@yonsei.ac.kr (S. Jeong).

http://dx.doi.org/10.1016/j.compgeo.2014.07.009
0266-352X/

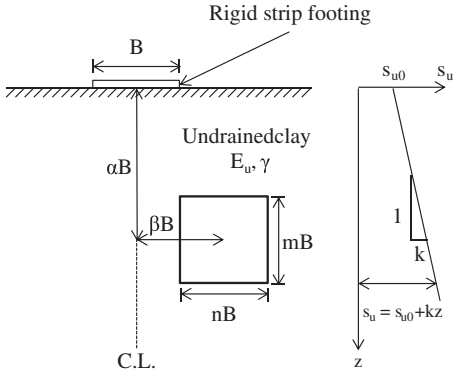

(a) Plane strain footing above single void

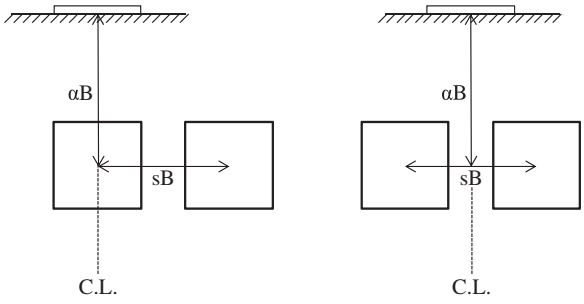

(b) Parallel configuration (c) Symmetrical configuration

Fig. 1. Problem definition (modified from Kiyosumi et al. [15]).

$$q_u = \frac{Q_u}{B} = s_u N_c \tag{1}$$

where q_u is the ultimate bearing stress on the footing, Q_u is the ultimate vertical force, B is the footing width, s_u is the undrained shear strength of the soil, and N_c is the dimensionless undrained bearing capacity factor.

This paper presents FE analyses for the calculation of the bearing capacity of surface strip footings on undrained clay with single and dual continuous voids. Consideration is given to the effects of void location, shape and number as well as soil rigidity and non-homogeneity. The results of the analyses are compared to other available solutions. Based on the analyses, design charts are presented in form of the undrained bearing capacity factor with respect to the dimensionless influencing parameters, and the governing failure mechanisms are discussed.

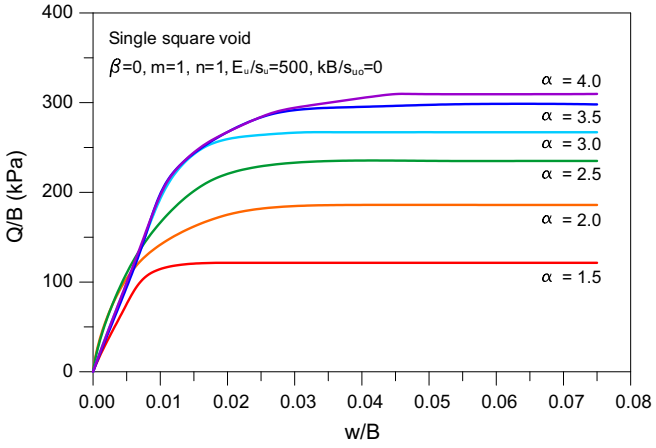

Fig. 3. Load–displacement curves for strip footing centered above single voids.

2. Problem definition

Fig. 1 illustrates the problem geometry studied and defines the key parameters. As shown in Fig. 1(a), a strip rigid footing of width B is placed on an isotropic, non-homogenous soil with a undrained Young's modulus E_u, a uniform unit weight γ, a surface undrained shear strength s_{u0}, and a rate of strength increasing with depth k. The undrained strength of the soil at a depth z is given as

$$s_u(z) = s_{uo} + kz \tag{2}$$

The undrained shear strength profile is common in normally consolidated (NC) clay, and $k = 0$ corresponds to the homogeneous clay with uniform strength. Such strength variation is quantified in terms of the nondimensional parameter kB/s_{uo}, which ranges typically between 0 and 1 for onshore applications [19,20].

The performance of a footing above voids is affected by the location, shape and number of voids [15], which are expressed through dimensionless parameters, i.e., the vertical void distance α (defined as the ratio of vertical distance from the ground surface to the

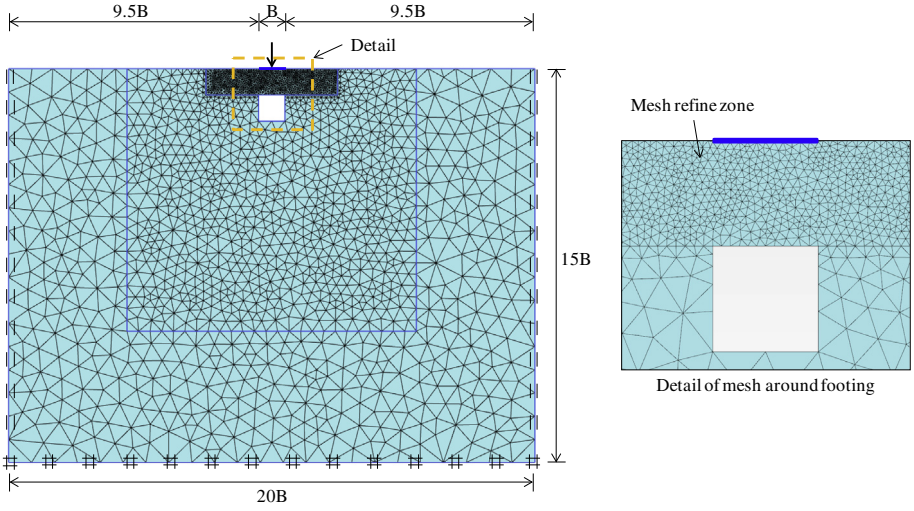

Fig. 2. Typical finite element mesh and boundary extension for soil and foundation domain.

center of the void), horizontal void distance β (defined as the ratio of the horizontal distance from the centerline of the footing to the center of the void), void width n (defined as the ratio of the void width to the footing width), and void height m (defined as the ratio of the void height to the footing width). The dual voids separated by the void spacing s (defined as the ratio of the center-to-center spacing of two voids to the footing width) are considered in this study, and their configuration is designed to two groups, i.e., parallel and symmetrical configurations, as shown in Fig. 1 (b) and (c), respectively.

3. Finite element analysis

Small strain finite element analyses of surface strip footings above voids were carried out using a commercially available Plaxis 2D Version 2012 [21]. The soil was modeled with fifteen-node triangular elements while the footing was composed of six-node triangular plate elements that are compatible with triangular side of the degenerated soil elements.

The soil surrounding the voids was modeled as a Tresca material using the elastic-perfectly plastic Mohr–Coulomb failure criteria. Poisson's ratio of $\nu = 0.495$ and friction and dilation angles of $\phi = \psi = 0$ were set to simulate the undrained clay. The undrained Young's modulus and bulk unit weight were assumed to be $E_u = 30$ MPa and $\gamma = 20$ kN/m^3, respectively. It is worth noting that the undrained bearing capacity of a surface footing resting on level ground is insensitive to the soil unit weight [22]. The three different values of undrained shear strength of the soil were taken as s_u = 60, 100 and 300 kPa, and the soil rigidity E_u/s_u was constant, irrespective of depth. The footing was modeled as a non-porous linear elastic material with 1 m thickness and Young's modulus for concrete $E_c = 30$ GPa. The geostatic stress was generated by taking the coefficient of earth pressure at rest, $K_0 = 1$.

Fig. 2 shows a typical finite element (FE) mesh and boundary extensions of the soil domain for the plain strain surface footing. The external boundaries were positioned 9.5B laterally from the edge of the foundation and 15B below the ground surface, which minimizes possible boundary effect on the predicted bearing capacity. Zero horizontal displacements were prescribed at the lateral boundaries and full fixities at the bottom boundary. The voids were introduced by excavation of the soil at the designed depth for each analysis. Since the mesh density in the area adjacent to the footings, particularly at level ground, is of most importance for the bearing capacity factor calculation, element density was increased in this area. The optimum size and distribution of elements were taken to be obtained when further modification of elements did not provide a further reduction in the value of bearing capacity factor calculated. The total number of elements varied from 3003 to 5235, depending on geometrical parameters.

No special interface elements along the soil and footing interface were used, indicating that the footing was simulated as rough with the same shear strength and shear modulus for the interface and adjacent soil elements. Instead, to allow an effective gap to form between part of the footing and the soil, a very thin 0.03 m zone of zero tensile strength soil elements was modeled beneath

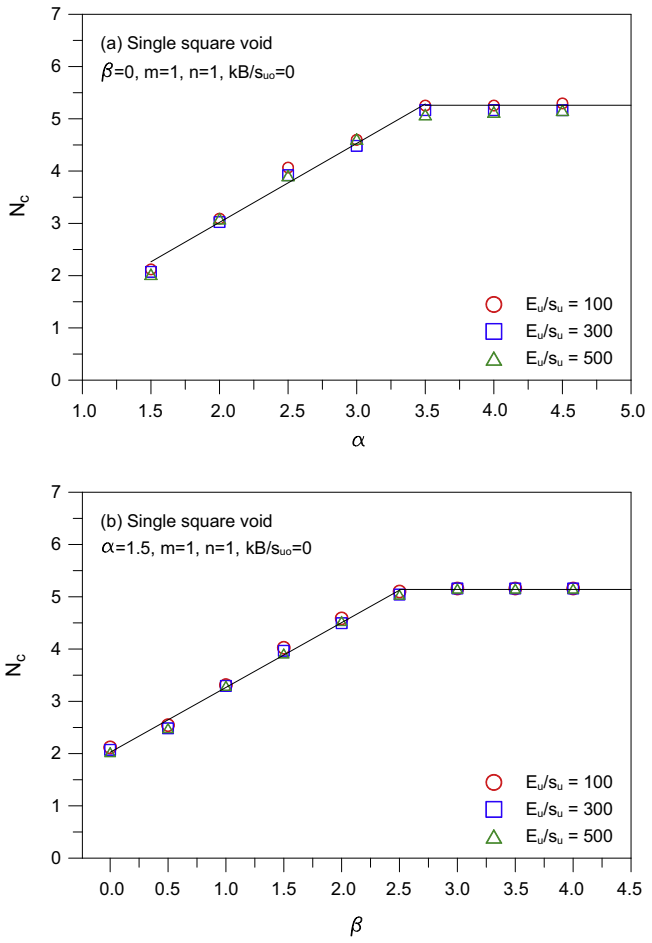

Fig. 4. Effect of soil rigidity on bearing capacity factor of strip footings above single voids.

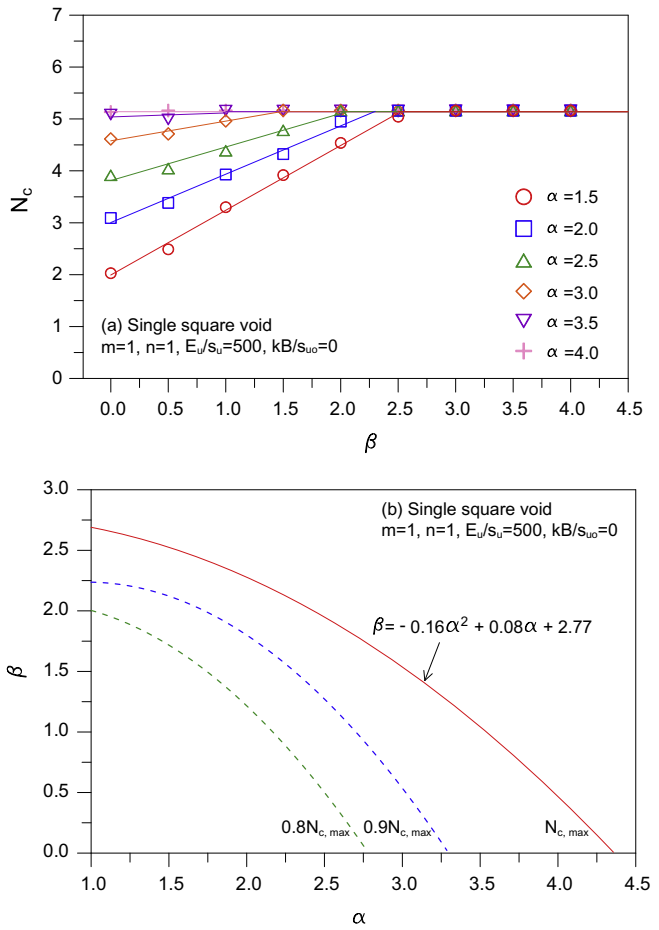

Fig. 5. Bearing capacity factor of strip footings above single voids and their critical void locations.

the footing, indicating that the interface elements cannot sustain tension [23].

Fig. 3 shows the typical normalized load–displacement curves for the footings centered above voids (i.e., $\beta = 0$), where w represents the displacement of the footings corresponding to the mobilized vertical force Q. For all cases, the footing reaches a clear limit load, which was taken as the ultimate bearing capacity.

4. Results and discussion

Fig. 4 shows the effect of soil rigidity on the bearing capacity factor of strip footings above single square voids. The soil rigidity has little influence on the capacity factor, irrespective of the void location. It is noted that the bearing capacity of a surface footing resting on ground is independent of the soil rigidity [24]. The soil rigidity is taken as $E_u/s_u = 500$ for further numerical calculations. The results also indicate that the influence of void location on the footing bearing capacity decreases as the distance between the void and footing increases, and there exists a certain location beyond which the void effect on the undrained stability of the footing become negligible, as described by Baus and Wang [8]. Fig. 4(a) shows that for a given value of $\beta = 0$, the capacity factor increases linearly with the value of α up to a limiting value, defined as the maximum bearing capacity factor $N_{c,\max}$. The value of $N_{c,\max}$ obtained from the current FE analyses is 5.16, which is 0.4% higher than the Prandtl solution of $2 + \pi$. A similar variation of capacity factor with respect to β for a constant value of $\alpha = 1.5$ is shown in Fig. 4(b). The values of the capacity factors for $\beta = 0$ and $\alpha = 1.5$ can be approximated by the following equations:

$$N_c = 1.47\alpha \leqslant N_{c,\max} \tag{3}$$

$$N_c = 1.26\beta + 2.00 \leqslant N_{c,\max} \tag{4}$$

Fig. 5(a) shows the variation of the bearing capacity factor of strip footing with β for different values of α. The capacity factor increases with an increase in the value of α, but the capacity factor with lower α significantly increases with the value of β. It is also found that the value of β_{cr}, representing the critical void eccentricity at which the capacity factor becomes equal to the maximum bearing capacity factor, decreases with increasing the value of α. From Fig. 5(a), the critical void location is determined, which is denoted by the solid line in Fig. 5(b). When the void is located above the line, the existence of the void can be ignored, implying that the capacity factors are same as $N_{c,\max}$. When the void is located below the line, however, the capacity factor varies with the void location, obviously less than the value of $N_{c,\max}$. The equivalent lines of the capacity factors with $0.9N_{c,\max}$ and $0.8N_{c,\max}$ are represented by the dotted lines in Fig. 5(b).

Fig. 6 shows the bearing capacity factor of strip footings centered above the single rectangular voids that are wider than they are high. Fig. 6(a) shows the results for void cases with varying the void width parameter n but the constant void height parameter of $m = 1$. At a given value of α, the capacity factor normally decreases as the value of n increases. The rate of reduction in capacity factor is insensitive to the overall value of α, particularly for the value of $n > 1.5$. Fig. 6(b) shows the results for void cases with different combinations of n and m but the constant area of the cross-section, i.e., $mn = 1$. At a given value of α, the capacity

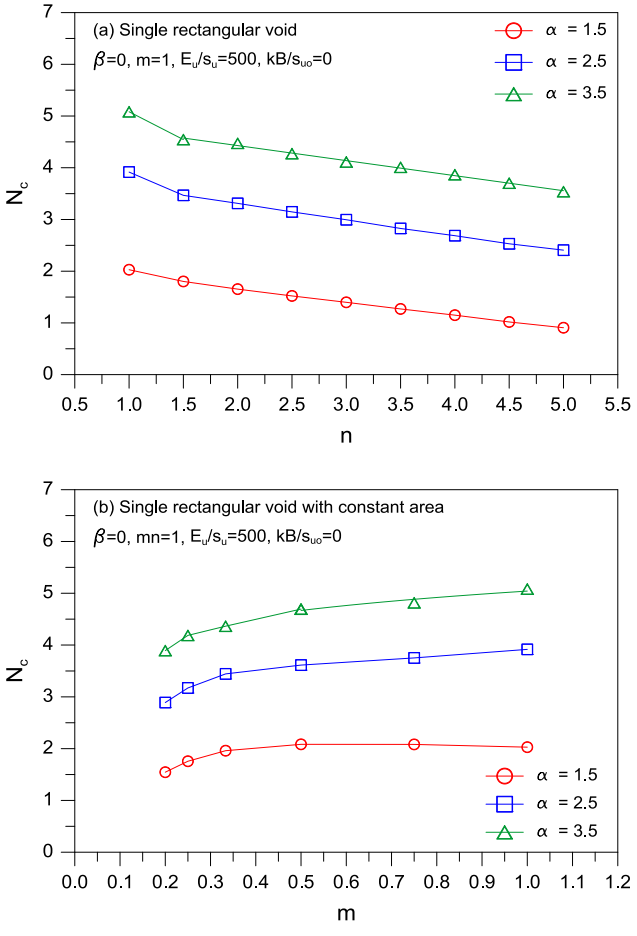

Fig. 6. Bearing capacity factor of strip footings above single rectangular voids.

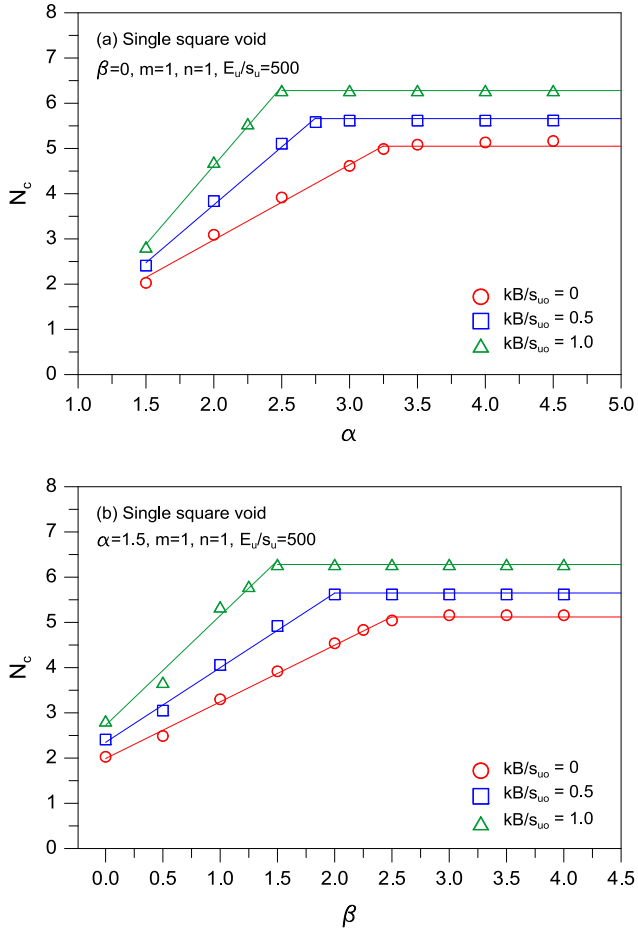

Fig. 7. Bearing capacity factor of strip footings on inhomogeneous clay with single voids.

factor is found to increase gradually with an increase in the value of m.

Fig. 7 shows the variation of bearing capacity factor as a function of soil non-homogeneity for given values of α and β. As expected, the greater value of kB/s_{uo} gives the higher capacity factor. Furthermore, the maximum bearing capacity factor increases continuously with an increase in the value of kB/s_{uo}. For $kB/s_{uo} = 0.5$ and 1, the maximum bearing capacity factors of Skempton [25] are estimated to be 5.83 and 6.67, respectively. Another solution obtained using the method of characteristics [26] is 5.79 and 6.47, respectively. The corresponding values of $N_{c,\max}$ by the current FE analysis are lower than the existing solutions. Meanwhile, the critical void location generally decreases with increasing the value of kB/s_{uo}.

Fig. 8 shows the bearing capacity factor of strip footings above dual square voids. The results reveal that regardless of the void configuration (i.e., parallel and symmetrical configurations), the capacity factor increases as the two voids are moved further apart. This is attributed to the higher shear resistance provided by a wider pillar between the adjacent voids. Fig. 8(a) shows that for all vertical void distance parameter except for $\alpha = 4.5$, the capacity factor increases with the value of s and reaches at a certain value, identical to the capacity factor for single void cases shown in Fig. 4(a). Fig. 8(b) shows that the capacity factor increases with increasing the value of s, although this trend is predominant at the lower values of α. In general, as the value of s increases, the rate of increase in capacity factor first increases, then decrease and eventually approaches zero. It is noteworthy that the footing bearing capacity for dual square voids with $s = 1$ becomes equal to that of single rectangular voids with the combination of $n = 2$ and $m = 1$.

From Fig. 8, the critical spacing of dual voids with the parallel and symmetrical configurations is determined and plotted in Fig. 9(a). The critical spacing is the spacing beyond which the capacity factor becomes equals to unity, indicating no interference effect. For the parallel configuration, the critical spacing is not affected by the value of α. For the symmetrical configuration, however, the critical spacing linearly decreases with increasing the value of α. Fig. 9(b) compares the bearing capacity factors for the parallel and symmetrical dual-void configurations, together with the result for the single void cases shown in Fig. 4(a). For all values of α and s, the capacity factor for the single void cases is higher than that for the dual void with parallel configuration. It is also found that the symmetrical configuration has higher capacity factor compared to the parallel configuration, and their difference is higher at the lower values of α and the higher values of s.

Fig. 10 illustrates the FE displacement contours at collapse for strip footings above single voids in homogeneous clay. The failure mode is strongly dependent on the location and shape of voids. For shallow square voids, the estimation of collapse loads are given by the roof failure mechanism, characterized by the downward movement of a rigid soil block immediately above the void. Fig. 10(a) shows a typical type of the roof failure for the shallowest square void ($\alpha = 1.5$, $m = 1$, and $n = 1$). As the void location is vertically and horizontally farther from the footing, the collapse mode becomes wider and deeper, and involves the combination of the roof and wall failure mechanisms (Fig. 10(b)–(d)). For the shallow

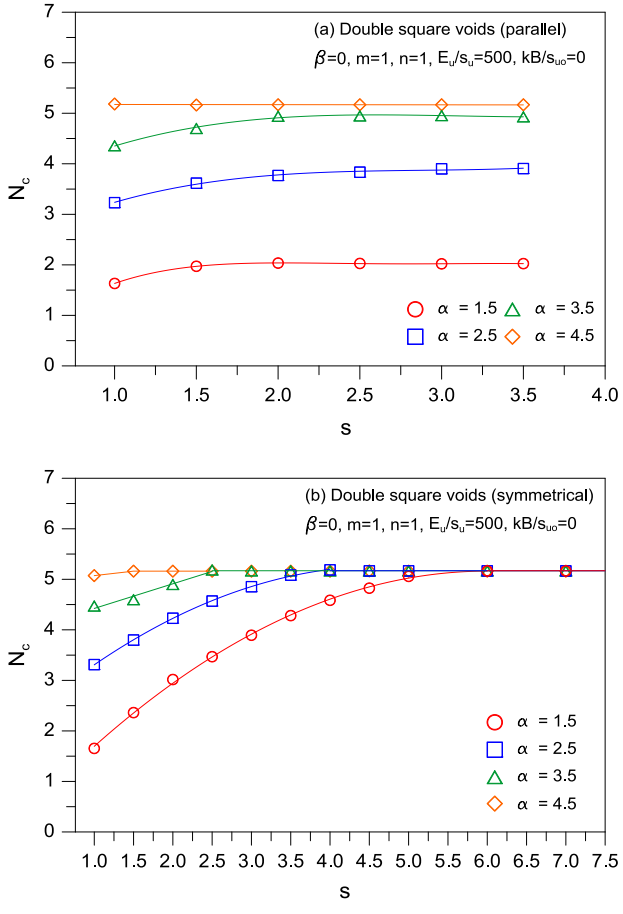

Fig. 8. Bearing capacity factor of strip footings above dual voids.

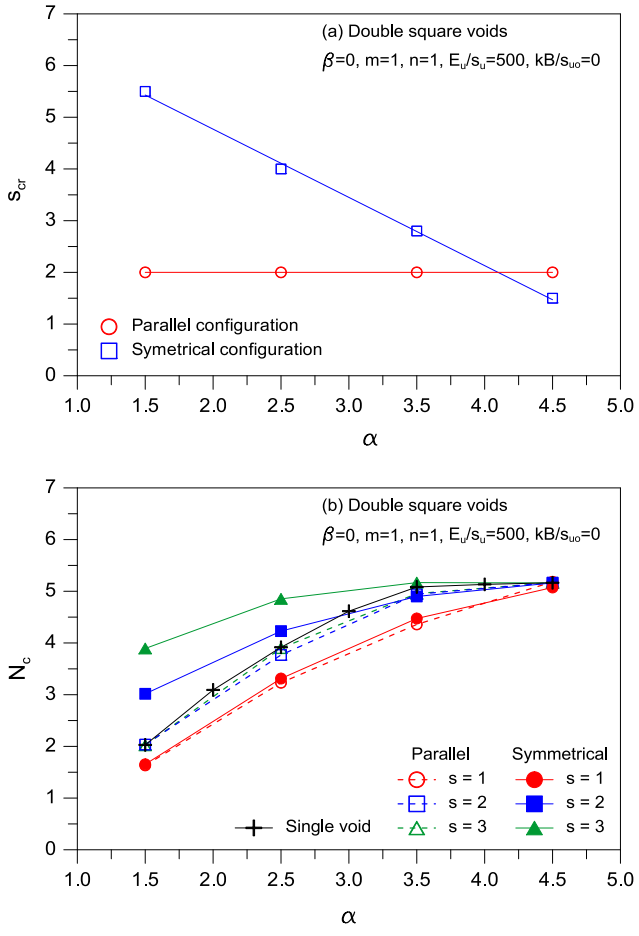

Fig. 9. Comparisons of critical spacing ratio and undrained bearing capacity for dual voids with parallel and symmetrical configurations.

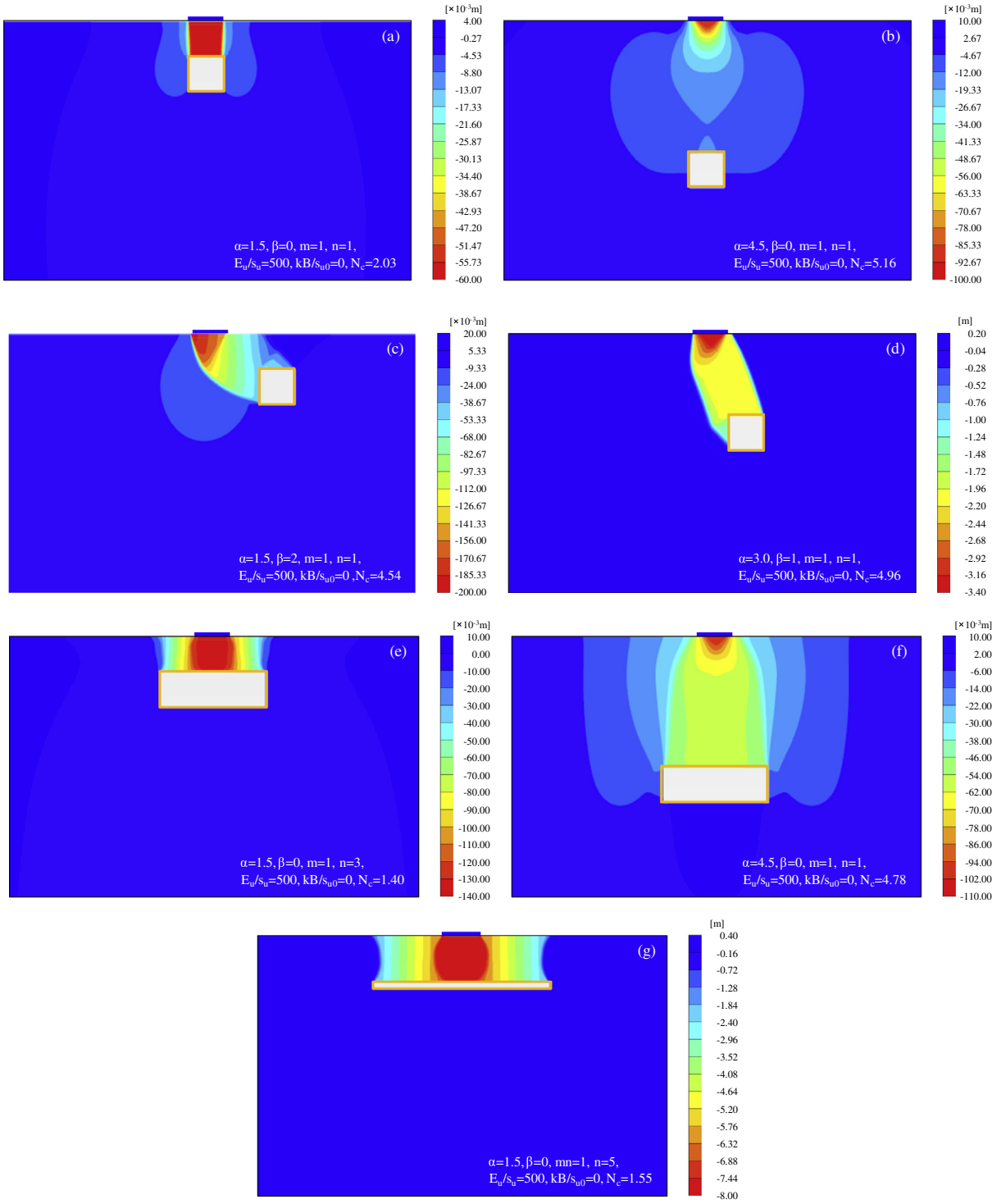

Fig. 10. FE displacement contours for strip footings above single voids.

rectangular void ($\alpha = 1.5$, $m = 1$, and $n = 3$), the failure pattern is more complex than the simple roof failure mechanism and includes the soil mass rotation (Fig. 10(e)). For the moderately deep rectangular void ($\alpha = 4.5$, $m = 1$, and $n = 3$), the failure mode constitutes roof and wall movement and the boundaries of the plastic zone extends laterally outward (Fig. 10(f)). Fig. 10(g) shows the collapse mechanism for the shallow rectangular void ($\alpha = 1.5$, $mn = 1$, and $n = 3$), which is similar to that shown in Fig. 10(e) but higher ration of soil mass above the void. The failure mechanisms shown in Fig. 10 are similar to the previous observation from the upper bound theorem of limit analysis in the work by Kiyosumi et al. [16].

Fig. 11 illustrates the FE displacement contours for strip footings above dual voids in homogeneous clay. The soil displacement near each void overlapped, which causes the reduction in bearing capacity, as shown in Figs. 11(a) and (b). When the void spacing is large enough, however, the interaction between the voids does not affect the footing performance. In particular, for the parallel configuration cases, the footing behaves and collapse as single void cases. The displacement patterns also show that for the parallel

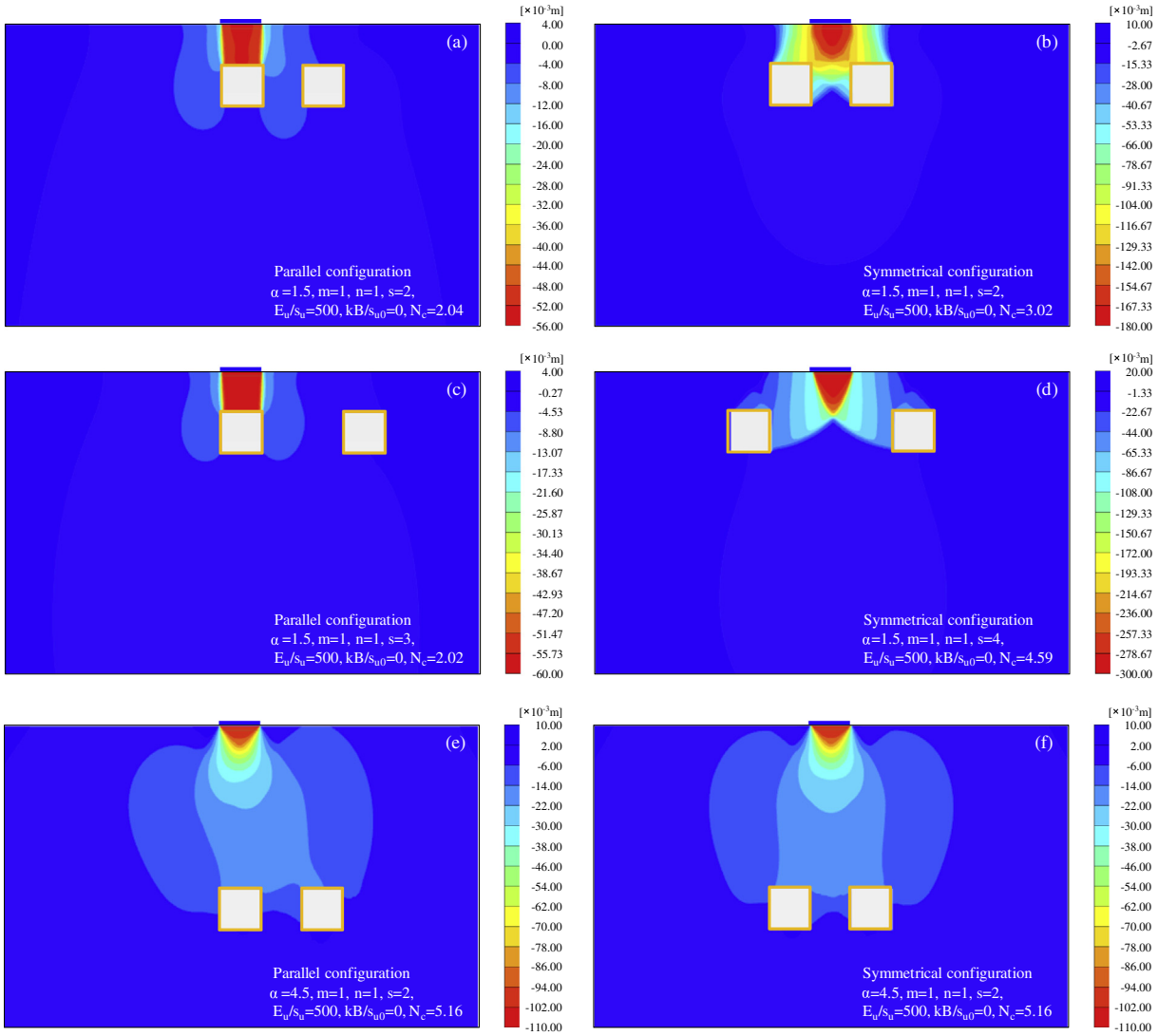

Fig. 11. FE displacement contours for strip footings above dual voids.

configuration cases, the pillar between the two voids is not supporting much of the vertical load. For the symmetrical configuration cases, however, the pillar carries a substantial amount of load and the clear combined failure mechanism of roof and wall is observed. This phenomenon suggests that the negative effect of dual voids is more prominent at the symmetrical configuration than at the parallel configuration, which is consistent with the results shown in Fig. 9(b). The relationship between the failure mode and the horizontal and vertical void distances from the footing is also shown in Fig. 11(c)–(f).

5. Conclusions

The undrained stability of surface strip footing on clay with continuous voids has been investigated. By using small strain finite element analysis (Plaxis [21]), the undrained vertical bearing capacity factor of footings for various geometrical and material parameters has been calculated. The validation is performed by comparing the existing solutions for undrained clay without voids. The following conclusions can be drawn from the present study:

(1) For single square voids, the bearing capacity factor increases linearly with increasing the vertical and horizontal void distances (α and β) up to a certain critical void location (α_{cr} and β_{cr}) beyond which the capacity factor becomes constant. There exists a critical curve beyond which the effect of void on the undrained stability of the footings becomes negligible.

(2) For footing centered above single rectangular voids, the bearing capacity factor for given value of α generally decreases with increasing the void width.

(3) The soil rigidity has little effect on the bearing capacity factor, regardless of void location. For non-homogenous clay, the values of α_{cr} and β_{cr} decreases with an increase in the value of kB/s_{u0}: the parameter quantifies the rate of the undrained strength increasing with depth. The capacity factor for given values of α and β is found to increase continuously with an increase in kB/s_{u0}.

(4) For dual voids, the bearing capacity factor decreases with decreasing the spacing between the two voids. The reduction in the capacity factor resulting from the interference effect is more pronounced at the symmetrical configuration than the parallel one. It is has been shown that to eliminate the interference effect of the voids, the spacing between the two void requires to be higher than a certain critical spacing s_{cr}. For the symmetrical configuration, the value of s_{cr} decreases continuously with an increase in α. For the parallel configuration, however, the value of s_{cr} is independent of α.

(5) Three distinct types of failure modes are observed in the FE displacement contour at the collapse: roof, wall, and combined failure mechanisms, which are similar to the previous results from upper bound solution of limit analysis in the literature.

Conflict of interest

The authors declare that there is no conflict of interest.

Acknowledgments

The authors acknowledge support in this research for the National Research Foundation of Korea (NRF) (Grant Nos. 2011-0030040 and 2013R1A6A3A01023199).

References

[1] Andersland OB, Ladanyi B. An introduction to frozen ground engineering. 2nd ed. New Jersey: John Wiley and Sons; 2004.
[2] Tharp TM. Mechanics of upward propagation of cover collapse sinkhole. Eng Geol 1999;52:23–33.
[3] Fam MA, Cascante G, Dusseault MB. Large and small strain properties of sands subjected to local void increase. J Geotech Geoneviron Eng 2002;128:1018–25.
[4] Park S. Effect of large void formation on strength of cemented glass beads. Eng Geol 2012;26:75–81.
[5] Espinoza DN, Kim SH, Santamarina JC. CO_2 geological storage – geotechnical implications. KSCE J Civil Eng 2011;15:707–19.
[6] Hillel D. Encyclopedia of soils in the environment, vol. 1. New York: Academic Press; 2004.
[7] Waltham T, Bell F, Culshaw M. Sinkholes and subsidence, karst and cavernous rocks in engineering and construction. New York: Springer; 2005.
[8] Baus RL, Wang MC. Bearing capacity of strip footings above void. J Geotech Eng 1983;109:1–14.
[9] Badie A, Wang MC. Stability of spread footing above void in clay. J Geotech Eng 1984;110:1591–605.
[10] Wang MC, Badie A. Effect of underground void on foundation stability. J Geotech Eng 1986;111:1008–19.
[11] Wood LA, Larnach WJ. The behavior of footings located above voids, vol. 4. In: Proc 11th int conf soil mech found eng; 1985. p. 273–6.
[12] Wang MC, Hsieh CW. Collapse load of strip footing above circular void. J Geotech Eng 1987;113:511–5.
[13] Al-Tabbaa A, Russell L, O'Reilly M. Model tests of footings above shallow cavities. Ground Eng 1989;22:39–42.
[14] Sreng S, Ueno K, Mochizuki A. Bearing capacity of ground having a void. In: 57th JSCE annual meeting; 2002. p. 1221–2 [in Japanese].
[15] Kiyosumi M, Kusakabe O, Ohuchi M, Peng FL. Yielding pressure of spread footing above multiple voids. J Geotech Geoneviron Eng 2007;133:1522–31.
[16] Kiyosumi M, Kusakabe O, Ohuchi M. Model tests and analyses of bearing capacity of strip footing on stiff ground with voids. J Geotech Geoneviron Eng 2011;137:363–75.
[17] Meyerhof GG. Some recent research on the bearing capacity of foundations. Can Geotech J 1963;1:16–26.
[18] Prandtl L. Uber die Harte Plasticher Korper. Nachr Ges Wiss. Gottingen Math Phys Kl 1920;12:74–85.
[19] Sloan SW, Assadi A. Undrained stability of a square tunnel in a soil whose strength in creases linearly with depth. Comput Geotech 1991;12:321–46.
[20] Osman AS, Mair RJ, Bolton MD. On the kinematics of 2D tunnel collapse in undrained clay. Geotechnique 2006;56:585–95.
[21] Brinkgreve RBJ, Engin E, Swolfs WM. Plaxis user's manual. Netherlands: Plaxis BV; 2012.
[22] Shiau JS, Merifield RS, Lyanmin AV, Sloan SW. Undrained stability of footings on slopes. Int J Geomech 2011;11:381–90.
[23] Georgiadis K. Undrained bearing capacity of strip footings on slopes. J Geotech Geoneviron Eng 2010;136:677–85.
[24] Chen Z, Tho KK, Leung CF, Chow YK. Influence of overburden pressure and soil rigidity on uplift on uplift behavior of square plate anchor in uniform clay. Comput Geotech 2013;52:71–81.
[25] Skempton AW. The bearing capacity of clays. Proc Build Res Cong. Division 1. Part 3; 1951. p. 180–9.
[26] Davis EH, Booker JB. The effect of increasing strength with depth on the bearing capacity of clays. Geotechnique 1973;23:551–63.